

Bayesian Multiresolution Modeling of Georeferenced Data

John Paige *

Department of Statistics, University of Washington,
Geir-Arne Fuglstad

Department of Mathematical Sciences, NTNU,
Andrea Riebler

Department of Mathematical Sciences, NTNU,
and Jon Wakefield *

Departments of Statistics and Biostatistics, University of Washington

May 27, 2020

Abstract

Current implementations of multiresolution methods are limited in terms of possible types of responses and approaches to inference. We provide a multiresolution approach for spatial analysis of non-Gaussian responses using latent Gaussian models and Bayesian inference via integrated nested Laplace approximation (INLA). The approach builds on ‘LatticeKrig’, but uses a reparameterization of the model parameters that is intuitive and interpretable so that modeling and prior selection can be guided by expert knowledge about the different spatial scales at which dependence acts. The priors can be used to make inference robust and integration over model parameters allows for more accurate posterior estimates of uncertainty.

The extended LatticeKrig (ELK) model is compared to a standard implementation of LatticeKrig (LK), and a standard Matérn model, and we find modest improvement in spatial oversmoothing and prediction for the ELK model for counts of secondary education completion for women in Kenya collected in the 2014 Kenya demographic health survey. Through a simulation study with Gaussian responses and a realistic mix of short and long scale dependencies, we demonstrate that the differences between the three approaches for prediction increases with distance to nearest observation.

Keywords: Spatial analysis; Extended LatticeKrig; Latent Gaussian models; Bayesian inference; Integrated Nested Laplace Approximations.

*John Paige was supported by The National Science Foundation Graduate Research Fellowship Program under award DGE-1256082, and Jon Wakefield was supported by the National Institutes of Health under award R01CA095994.

1 Introduction

The increasing size and complexity of spatial point datasets in fields such as climate sciences, public health, ecology, and social sciences have been concurrent with methodological developments in spatial statistics. While there are currently a host of methods available for handling inference with “big data” using traditional spatial models (Heaton et al., 2019), there has been less focus on accessible tools for more complex spatial dependence structures. In the context of multi-resolution spatial modeling, recent developments are the LatticeKrig (LK) model (Nychka et al., 2015) with the associated R package `LatticeKrig` (Nychka et al., 2016), and the multi-resolution approximation (M-RA) model (Katzfuss, 2017) with its implementation in the R package `GPvecchia` (Katzfuss and Guinness, 2020; Katzfuss et al., 2018; Zilber and Katzfuss, 2019). However, to the best of our knowledge there exist no Bayesian implementations of LK or M-RA allowing for non-Gaussian responses; `LatticeKrig` is limited to Gaussian responses as well, and `GPvecchia` allows general exponential families for the responses.

The most common approach to spatial modeling is to use parametric classes of spatial covariance functions with interpretable parameters such as the Matérn family. Depending on its smoothness parameter ν , the Matérn covariance class includes both exponential and Gaussian covariance functions. However, in practice, the smoothness parameter is commonly fixed at a small number, in part due to the difficulty in estimating this parameter, and the computational benefit of having one fewer parameter (Stein, 1999). It is known that, under infill asymptotics, it is the behavior of the Matérn covariance function at short spatial scales that most determines the likelihood and pointwise predictions (Stein, 1999, Ch. 3). This means that while short scale behavior of the Matérn covariance may be fit accurately, long scale correlations in the data will often not be accurately reproduced by the fit model. However, as we later show in the simulation study, long range correlations become increasingly important when making predictions far from observations. Additionally, we show in Appendix A that for areal predictions, errors in the covariances at spatial scales close to the average radius of the areas affect the uncertainty of those areal predictions the most, suggesting that long scale correlations are especially relevant when calculating the

uncertainty of areal averages for large areas.

The difficulty in identifying spatial model parameters makes it especially important to integrate over uncertainty when calculating predictive uncertainty. In a frequentist setting the bootstrap can be applied, but it relies on asymptotics and is computationally expensive since it requires the model to be refit many times (Sjöstedt-de Luna and Young, 2003). Handcock and Stein (1993) and Gelfand et al. (2010, Ch. 3.7) recommend using Bayesian inference in spatial statistics due to the importance of accounting for uncertain covariance structure. However, Markov Chain Monte Carlo (MCMC) techniques are often difficult to implement with long running times and large memory requirements, especially with large numbers of observations (Filippone et al., 2013). Detailed output diagnostics are also necessary to assess convergence.

As such, the key limitation in providing Bayesian inference for multiresolution spatial models is the computational complexity involved. In this paper, we propose to take advantage of the deterministic algorithm for Bayesian inference based on Integrated Nested Laplace Approximations (INLA) (Rue et al., 2009b). LK uses different layers of compact basis functions together with an associated sparse precision matrix, and fits directly into the INLA framework of latent Gaussian models. We provide an implementation using the R package INLA, which permits fast and accurate estimation of posterior marginal densities provided that the number of parameters is not too big (typically 2 to 5, but not exceeding 20 (Rue et al., 2017)). This extended version of LK is termed extended LatticeKrig (ELK). A key change from the original LK formulation is a reparametrization that improves interpretability and facilitates modeling and prior selection. Furthermore, the INLA implementation means that the ELK spatial model can be fit jointly with other random effects such as models for temporal trends or nonlinear covariate effects, handle non-Gaussian responses, integrate over parameter uncertainty, and incorporate prior knowledge through expert knowledge and/or for the purpose of robustness.

We will contrast ELK to traditional spatial models using the stochastic partial differential equation (SPDE) approach (Lindgren et al., 2011) as implemented in INLA to permit fast Bayesian approximate inference for latent Gaussian models where the tradi-

tional Matérn covariance function is used for spatial modeling (Lindgren and Rue, 2015). In this context, the SPDE approach is only one choice among many others for making the computations possible: employing low rank covariance matrices (Cressie and Johannesson, 2008; Banerjee et al., 2008; Finley et al., 2009), sparse covariance matrices (Knorr-Held and Raßer, 2000; Sang and Huang, 2012; Konomi et al., 2014; Neelon et al., 2014; Furrer et al., 2006; Hirano and Yajima, 2013), sparse precision matrices (Nychka et al., 2015; Katzfuss, 2017; Katzfuss and Hammerling, 2017; Lindgren et al., 2011; Datta et al., 2016a,b; Guinness, 2019; Guinness and Fuentes, 2017), or algorithmic approaches (Gerber et al., 2018; Guhaniyogi and Banerjee, 2018; Gramacy and Apley, 2015).

In Section 2 we introduce the main application on prevalence of secondary education for women in Kenya that motivated this work. In Section 3 we describe LK and ELK. We evaluate ELK, LK, and a SPDE model in a simulation scenario when fit to random fields with mixtures of short and long-range correlations in Section 4. In Section 5 the ELK and SPDE models are applied to the real data introduced in Section 2, and their predictive performance is assessed. Section 6 concludes this work with a discussion.

2 Motivating application

Sustainable Development Goal (SDG) 4 (United Nations, 2020) calls for improvements in secondary education to the point where everyone can complete their secondary education by 2030 regardless of their gender or the place where they live. Reliable spatial estimates of secondary education completion for young women are of particular importance to SDG 4. Yet in many developing countries, estimates of secondary education completion rely on complex, multistage household surveys (Li et al., 2019; Wagner et al., 2018) such as demographic health surveys (DHS) (USAID, 2019), multiple indicator cluster survey (MICS) (UNICEF - Statistics and Monitoring, 2012), AIDS indicator surveys (AIS) (DHS Program, 2019), and living standard measurement surveys (LSMS) (The World Bank, 2019).

Often, these household surveys are stratified by administration area and urbanicity; see for instance ICF International (2012). However, the classifications of urban or rural for the sampled clusters was made at the time of the last census, which at best takes place

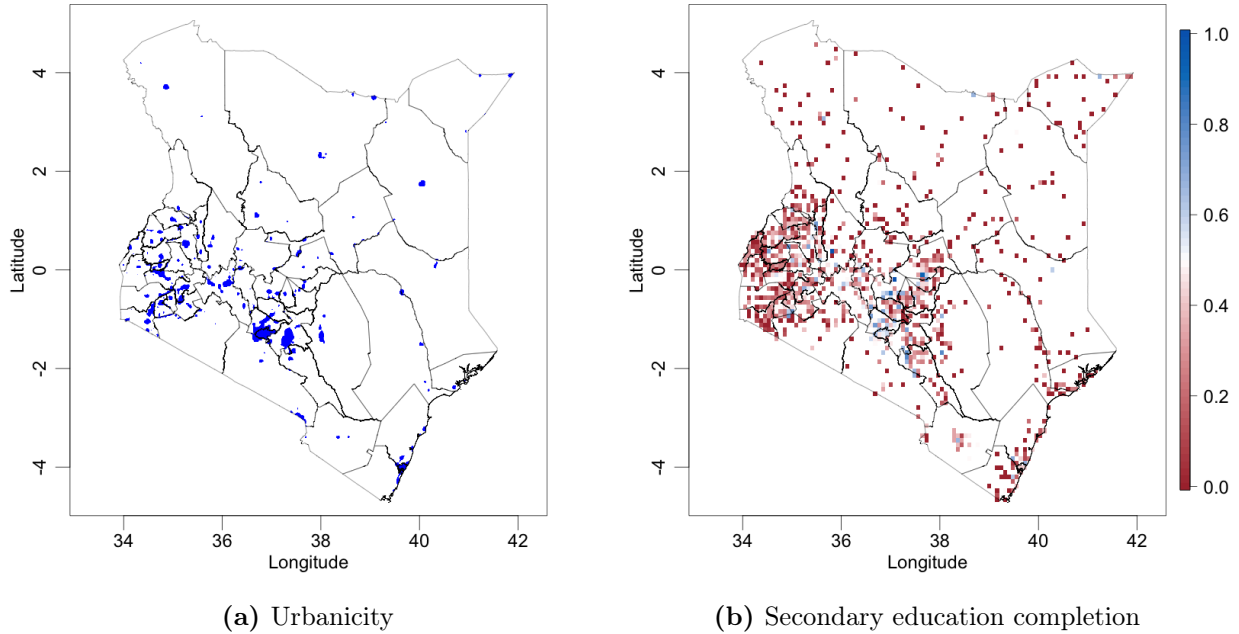


Figure 1: (a) Map of binary urbanicity classification in Kenya, and (b) 2014 empirical proportion of women aged 20-29 in Kenya that completed their secondary education.

every 10 years, and the specific continuous spatial classifications of urbanicity used in the censuses are generally not made publicly available. This forces modelers to either ignore urbanicity or assume that the classification remains accurate over large time spans, and to estimate urbanicity for unobserved locations based on proxy data such as population density (Paige et al., 2020; Wakefield et al., 2019). Because administrative areas are relevant for stratification in household surveys, and also since household surveys are often used to calculate population averages in administrative areas for policymakers, any spatial model used in this context must be able to simultaneously produce accurate averages in areas of varying size. Such models will therefore need to accurately estimate correlations at all spatial scales relevant for the sizes of the areas over which averages are calculated, and account for the uncertainty in those correlation estimates.

In this work we consider prevalence of secondary education completion for young women in Kenya in 2014. Data are obtained from the 2014 Kenya DHS (KDHS, 2014) consisting of 1,612 clusters, each with official urban/rural designations, and age and educational achievement information for the sampled women within the cluster. The modeled response

is the number of women aged 20-29 that have completed their secondary education. Paige et al. (2020) found that there are large differences in secondary education completion between urban and rural areas, and Figure 1 shows that urbanicity changes sharply over short spatial scales. This motivates the development of spatial models that can include spatial dependence at widely different spatial scales. We revisit this dataset in Section 5 to explore the sensitivity of spatial analysis to the inclusion or non-inclusion of an urban covariate, and the degree to which the ELK model can guard against spatial oversmoothing when urbanicity is not included and how well short and long scale correlations are captured when urbanicity is included.

3 Methods

3.1 Background on LatticeKrig

Nychka et al. (2015) introduced LK as a computationally efficient method for spatial modeling the stochastic process $Y = \{y(\mathbf{x}) : \mathbf{x} \in \mathcal{D}\}$ for spatial domain \mathcal{D} measured at observation locations $\mathbf{x}_1, \mathbf{x}_2, \dots, \mathbf{x}_n \in \mathbb{R}^2$. The observation model was assumed to be Gaussian, with $y(\mathbf{x}_i) | \eta_i, \sigma_N^2 \sim \mathcal{N}(\eta_i, \sigma_N^2)$, $i = 1, \dots, n$, where $\boldsymbol{\eta} = (\eta_1, \eta_2, \dots, \eta_n)$ were the linear predictors and σ_N^2 was the nugget variance. The linear predictors were assumed to follow a linear model $\boldsymbol{\eta} = \mathbf{Z}\boldsymbol{\beta} + \mathbf{u}$, where \mathbf{Z} is a $n \times p$ matrix where each column specifies a covariate, $\boldsymbol{\beta} = (\beta_1, \beta_2, \dots, \beta_p)^T$ is a vector containing the coefficients associated with the covariates, and $\mathbf{u} = (u(\mathbf{x}_1), u(\mathbf{x}_2), \dots, u(\mathbf{x}_n))$ are the values of the spatial Gaussian random field (GRF) u at the observation locations.

LK is characterized by the decomposition of u into a series of lattices of increasing spatial resolutions over which increasingly fine basis functions are spaced,

$$u(\mathbf{x}) = \sum_{l=1}^L g_l(\mathbf{x}) = \sum_{l=1}^L \sum_{j=1}^{m(l)} c_j^l \phi_{l,j}(\mathbf{x}), \quad \mathbf{x} \in \mathcal{D} \subset \mathbb{R}^2.$$

Here L is a fixed, predetermined small number of lattice layers, usually between 2 and 4, and g_1, \dots, g_L are a series of smooth spatial functions associated with each lattice and composed of $m(1), \dots, m(L)$ basis functions respectively. Each g_l is respectively decomposed

into a linear combination of basis functions $\phi_{l,1}, \dots, \phi_{l,m(l)}$ with basis weights c_j^l , which are random variables.

Nychka et al. (2015) choose radial Wendland basis functions (Wendland, 1995), which have compact support. The basis functions are represented as $\phi_{l,j}(d) = \phi\left(\frac{d}{2.5\delta_l}\right)$, where $\phi(d) = (1-d)^6(35d^2 + 18d + 3)/3$ for $0 \leq d \leq 1$, and 0 otherwise. Here δ_l is the layer l lattice cell width, and the factor of 2.5 ensures that the radius of each basis function is 2.5 times the respective layer lattice cell width. This overlap reduces artifacts in the predictive spatial means and standard errors (Nychka et al., 2015).

The basis coefficients for each layer respectively follow independent SAR models with mean zero multivariate normal distribution, $\mathbf{c}_l \sim \text{MVN}(\mathbf{0}, \alpha_l \sigma_S^2 \mathbf{B}_l^{-1} \mathbf{B}_l^{-T})$, where α_l determines the proportion of spatial variance σ_S^2 attributed to layer l with $\sum_{l=1}^L \alpha_l = 1$, and \mathbf{B}_l is an autoregression matrix for layer l with elements $4 + \kappa_l^2$ on the diagonal and up to four additional non-zero elements on each row corresponding to each neighbor, and with values of -1 . As described in Lindgren et al. (2011), each layer l approximates a Gaussian process with Matérn covariance function having smoothness $\nu = 1$ and effective spatial range approximately $\rho_l \equiv \sqrt{8}\delta_l/\kappa_l$. Note that Nychka et al. (2015) achieves the desired spatial variance σ_S^2 in each point by numerical normalization of the covariance matrix. The interpretation of the α_l as proportion of variance attributed to layer l is not exact as the marginal variance of the different layers will vary depending on the values of κ_l .

Let \mathbf{A}_l be the $n \times m(l)$ regression matrix from the basis coefficients for layer l to the basis function values at the coordinates of the observations so that $(\mathbf{A}_l)_{i,j} = c_j^l \phi_{l,j}(\mathbf{x}_i)$. We can then write the regression matrix from all basis coefficients to the values of the basis functions at the observation locations as $\mathbf{A} = (\mathbf{A}_1 \dots \mathbf{A}_L)$ so that $\mathbf{u} = \mathbf{A}\mathbf{c}$, where $\mathbf{c} = (\mathbf{c}_1^T \dots \mathbf{c}_L^T)^T$. This means that the linear predictor can be written as $\boldsymbol{\eta} = \mathbf{Z}\boldsymbol{\beta} + \mathbf{A}\mathbf{c}$.

In the above formulation, LK requires p parameters for fixed effects, and $2L + 1$ parameters for the covariance including the spatial variance σ_S^2 , error variance σ_N^2 , $L - 1$ parameters for the layer weights, and L effective range parameters. It is sometimes assumed for simplicity that $\kappa_1 = \kappa_2 = \dots = \kappa_L$, in which case the effective range of each layer is controlled exclusively by the layer resolution. Under this assumption, LK requires

only $L + 2$ covariance parameters.

3.2 A Bayesian extension to latent Gaussian models

We make two major additions to the formulation in the previous section: we allow for the model to be fit jointly with other structured random effects, and we allow for non-Gaussian responses. The model for the linear predictor is extended to $\boldsymbol{\eta} = \mathbf{Z}\boldsymbol{\beta} + \mathbf{A}\mathbf{c} + \sum_{i=1} \mathbf{M}_i\boldsymbol{\gamma}_i$, where the matrices \mathbf{M}_i are fixed and define a mapping to the observations from random effects collected in the vectors $\boldsymbol{\gamma}_i$ such as temporal trends, space-time interactions, and other modeled effects. The vector $\boldsymbol{\gamma} = (\boldsymbol{\gamma}_1^T, \dots, \boldsymbol{\gamma}_m^T)^T$ is assumed to follow a joint Gaussian distribution. Denote by $\boldsymbol{\theta}_M$ and $\boldsymbol{\theta}_L$ the vectors containing all model and family likelihood hyperparameters respectively. We can then formulate a latent Gaussian model in three stages. In stage 1, we have conditionally independent observations that may be non-Gaussian with likelihood $\pi(\mathbf{y}(\mathbf{x}_i)|\boldsymbol{\eta}_i, \boldsymbol{\theta}_L)$, $i = 1, 2, \dots, n$. In stage 2, the latent model is a joint Gaussian distribution for $(\boldsymbol{\beta}, \boldsymbol{\gamma}, \mathbf{c})|\boldsymbol{\theta}_M$. Lastly, in stage 3, we assign a prior $\pi(\boldsymbol{\theta})$, where $\boldsymbol{\theta} = (\boldsymbol{\theta}_M, \boldsymbol{\theta}_L)$.

To better understand the $\sum_{i=1} \mathbf{M}_i\boldsymbol{\gamma}_i$ term, and to see why it adds so much generality to ELK, we could consider the relatively simple example of modeling a set of T repeated observations of n spatial locations through time points $t = 1, \dots, T$. If our covariates aside from β_0 , the intercept, can be split into one set of covariates changing only in space and one set of covariates changing only in time, we could then model the fixed effects in space and time as $\mathbf{Z}_S\boldsymbol{\beta}_S$ and $\mathbf{Z}_T\boldsymbol{\beta}_T$ respectively for $n \times p_S$ matrix \mathbf{Z}_S and $T \times p_T$ matrix \mathbf{Z}_T . Similarly, we might assume that the spatial random effect varied only in space and the temporal random effect varied only in time. If the temporal trend is AR(1), then we can set $\boldsymbol{\gamma} \sim \text{AR}(1)$, for a T dimensional vector $\boldsymbol{\gamma}$. We could then define the model as, $\boldsymbol{\eta} = \mathbf{1}_{nT}\beta_0 + (\mathbf{1}_T \otimes \mathbf{Z}_S)\boldsymbol{\beta}_S + (\mathbf{Z}_T \otimes \mathbf{1}_n)\boldsymbol{\beta}_T + (\mathbf{1}_T \otimes \mathbf{A})\mathbf{c} + (\mathbf{I}_T \otimes \mathbf{1}_n)\boldsymbol{\gamma}$, where ‘ \otimes ’ represents the Kronecker product, and \mathbf{I}_T is a $T \times T$ identity matrix so that $\mathbf{M} = \mathbf{I}_T \otimes \mathbf{1}_n$ adds the coefficients of $\boldsymbol{\gamma}$ identically to the coefficients of $\boldsymbol{\eta}$ associated with the corresponding time point. This model can be fit in the ELK framework. Although not included in this model, interactions between the spatial and temporal effects could be included as well.

The key computational contribution of Rue et al. (2009a) is the combination of this formulation with the INLA approach to make Bayesian inference for the multiresolution latent Gaussian model computationally feasible. The combination is practically achieved by the implementation of the new model within the INLA package. We term the extended version of LatticeKrig, with computationally feasible inference, as extended LatticeKrig (ELK). Our implementation exploits `GMRFLib`-library (Rue and Follstad, 2001) functions for sparse symmetric positive definite matrices based on methods described in Rue and Held (2005) when generating the latent coefficient precision and covariance matrices, and also precomputes relevant matrices and normalization factors whenever possible. Details on computations involved in our ELK implementation are given in Appendix 6.

To ensure σ_S^2 can be approximately interpreted as the spatial variance and $(\alpha_1, \dots, \alpha_L)$ as the proportion of spatial variance attributed to the layers, we normalize separately the SAR processes associated with each layer so that the variance of each g_l in the center of the spatial domain is $\alpha_l \cdot \sigma_S^2$. This requires the computation of normalization constants $\omega_1, \dots, \omega_L$. Letting \mathbf{A}_l^* be the $1 \times m(l)$ regression row vector that maps the layer l basis coefficients to the value of the basis functions at the center of the spatial domain, each ω_l can be calculated as: $\omega_l = (\mathbf{A}_l^* \mathbf{B}_l^{-1} \mathbf{B}_l^{-T} (\mathbf{A}_l^*)^T)^{-1}$. This is different from LK, since we only normalize the process to have variance σ_S^2 in the center of the domain rather than at every point. This has the advantage that it is faster computationally, and we find that if the lattice resolutions and buffers are chosen using the method discussed in the following paragraph, then the resulting process has spatial variance close to σ_S^2 across the whole spatial domain. In order to avoid matrix inversion and quadratic form computations each time \mathbf{Q} is calculated, we precompute the mappings $f_l : \kappa_l \mapsto \omega_l$ using smoothing splines over a reasonable range of the values of κ_l .

In LK, the recommended setting for the layer resolutions are the relation $\delta_l = 2^{-(l-1)}\delta_1$, and when this relation is used in ELK under the assumption that $\kappa_1 = \dots = \kappa_L$, we call this the ‘fixed’ model (ELK-F). We propose to also consider a ‘tailored’ ELK model (ELK-T) with resolutions chosen for capturing variation at different spatial scales and with κ_l parameters allowed to vary for each layer. Since ELK-T allows the κ_l parameters to vary for

each layer, it requires $2L$ hyperparameters, whereas ELK-F requires $L + 1$ hyperparameters, although more would be required if other latent effects were included in the $\mathbf{M}\boldsymbol{\gamma}$ term or for any likelihood family hyperparameters. For both models, a conservative guideline is for lattice resolutions to be at most a fifth of the effective range of the corresponding layer to avoid lattice artifacts and for accurate interpretation of the layer’s effective range parameter. Since correlation lengths near the spatial domain diameter are very difficult to identify, we recommend choosing δ_1 to be finer than a fifth of the spatial domain diameter, and typically around a twenty fifth of the domain diameter, although the exact choice will depend on the context. Figure 8 in Section S.2 in the supplementary material illustrates how the lattices might be arranged for a specific problem. In the figure and in Section 4 we use a buffer of 5 cell widths to avoid edge effects due to the zero boundary condition for the basis coefficients of each layer. The buffer size can be adjusted depending on the estimated effective correlation range for that layer.

Expert knowledge on spatial scales at which dependence is expected could be used to choose appropriate resolutions in ELK-T. Furthermore, the Bayesian formulation allows the inclusion of expert knowledge when setting priors for the interpretable parameters. For simplicity, we suggest a Dirichlet distribution of order L for the proportion of variances assigned to each layer, that is $\boldsymbol{\alpha} \sim \text{Dirichlet}(a_1, \dots, a_L)$ with $a_l = 1.5/L$ for $l = 1, \dots, L$ in order to place equal weight in the prior on each layer, and to ensure the prior is slightly concave for the sake of identifiability. Since the chosen prior concentration parameter is 1.5, the Dirichlet prior is only slightly more concave than the flat Dirichlet distribution that would result if the concentration parameter were 1. On the spatial and nugget standard deviation we place penalized complexity (PC) priors satisfying $P(\sigma_S > 1) = 0.01$, although this will depend on the context and prior information. See Simpson et al. (2017) for details on PC priors.

We propose setting independent inverse exponential priors for the effective range in each layer, where the effective range for layer l is computed as $\rho_l = \sqrt{8}\delta_l/\kappa_l$. For ELK-T, we recommend beginning by placing a prior on one layer’s effective range, scaling priors for other layer effective range parameters proportionally to the lattice grid cell width δ_l

for ELK-T. For ELK-F, a single κ parameter is estimated so that $\kappa = \kappa_1 = \dots = \kappa_L$, and only one effective range parameter requires a prior. When placing priors on ELK-F or ELK-T effective ranges in this way, a prior on the effective range for one of the layers would therefore determine all effective range priors. Throughout this work, we set the median effective range of the coarsest layer at a fifth of the spatial domain diameter, determining any other effective range priors accordingly. However, the effective range priors can be customized to better suit the context as well the expert knowledge of the modeler.

A fully functional proof-of-concept implementation of ELK is freely available on Github at <https://github.com/paigejo/LK-INLA>. Since it is implemented in R and not natively in C++, it does not reach its full potential in terms of speed.

4 Assessing performance under multiscale dependence

4.1 Prediction quality measures

The different spatial models are compared using three measures of predictive performance: the root mean square error (RMSE), the continuous rank probability score (CRPS) (Gneiting and Raftery, 2007), and the empirical coverage of 80% prediction intervals. We also compared each model’s runtime including setup, model fitting, predictions, and predictive and covariance parameter uncertainty. For each model considered, we calculate the measures as an average of its values over each held-out observation. We consider two hold-out schemes: stratified randomized selection and holding out pre-specified regions. These are discussed in the section on the application. If observations are counts with denominator N_i for observation $1 \leq i \leq n$, then we rescale the counts to be empirical proportions with $y_i = y_i^*/N_i$ for observed count y_i^* .

Unlike RMSE, CRPS is a strictly proper scoring rule, and as such takes into account the accuracy of the central predictions as well as the calibration of the uncertainty. Smaller values are preferable. Prediction intervals at the 80% level are derived from the 0.1 and 0.9 quantiles of the predictive distribution. They are used to compute the prediction interval empirical coverage. For empirical proportions, and especially for small denominators, a

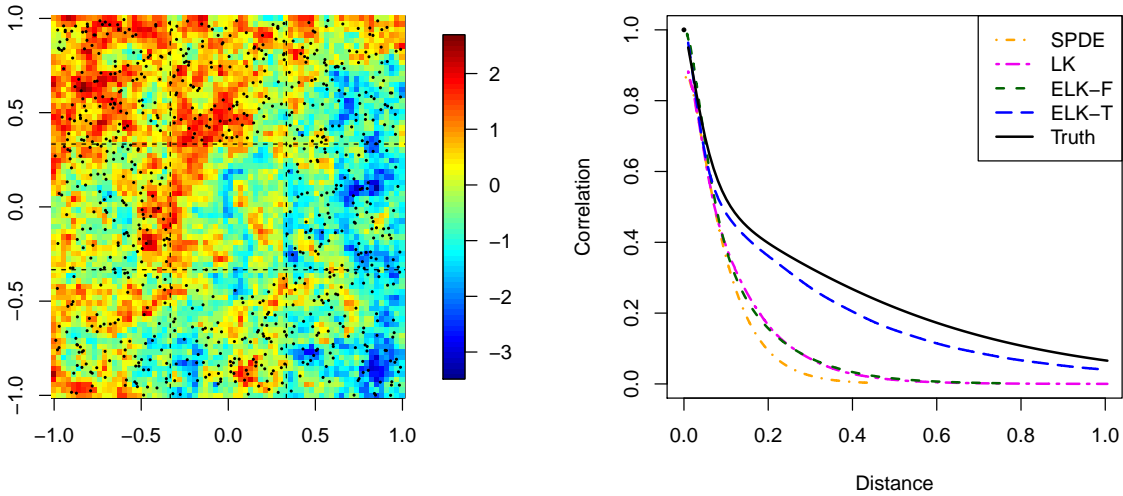
fixed prediction interval will generally not provide the correct coverage even if the predictive distribution is correct due to the discreteness of the sample space (Geyer and Meeden, 2005). We therefore follow Geyer and Meeden (2005) by calculating *fuzzy* coverage instead, with details given in Appendix S.1. We have found that fuzzy coverage is much more precise than non-randomized coverage, allowing us to be sure that observed over- or undercoverages are due to the accuracy of the predictive uncertainty rather than the discreteness of the CIs.

4.2 Simulation setting

We first simulate a spatial GRF u on the square $[-1, 1]^2$. The GRF has the covariance function $C(d) = 0.5(C_1^*(d; 0.08) + C_1^*(d; 0.8))$, where $C_1^*(d; \sigma_S^2) = (\sqrt{8}d/\rho)K_1(\sqrt{8}d/\rho)$ denotes the Matérn correlation (Stein, 1999) at distance d with smoothness $\nu = 1$ and effective spatial range ρ , and where K_1 is the modified Bessel function of the first order and second kind. The correlation function is plotted in Figure 2 along with an example realization. The domain is then subdivided into a regular 3×3 grid, and we draw 800 observations at random locations, $\mathbf{x}_1, \mathbf{x}_2, \dots, \mathbf{x}_{800}$, in the outer eight grid cells, but draw no observations within the central grid cell. We assume the unobserved latent process is $\eta_i = u(\mathbf{x}_i)$, and draw each observation $Y(\mathbf{x}_i)$ from $Y(\mathbf{x}_i)|\eta_i \sim \mathcal{N}(\eta_i, 0.1^2)$ for $i = 1, 2, \dots, 800$. We fit several models, which we will describe in the next section, to the data, and generate predictions of the spatial process Y on a fine 70×70 grid and predictions of areal averages of the process Y for the nine subdivision areas approximated numerically as averages of the values of Y on the 70×70 fine grid over each of the 9 areas. The whole procedure is repeated 100 times, and, for each realization, the predictions are scored in comparison to the truth. We choose to use Y as the process for comparing predictions rather than u so that comparison metrics are more similar to cross-validation, where only Y , and not u , is directly observed at the observation locations.

4.3 Models used in the simulation study

We use ELK-T with two layers: a grid of 14×14 basis knots and a grid of 126×126 knots over the spatial domain (not including the five knot buffer for each layer), which results in



(a) One realization of the spatial field

(b) True and estimated correlation functions

Figure 2: (a) One of the 100 spatial field realizations. Black dots indicate the 800 observation locations and dashed lines indicate the 3×3 grid used for areal predictions (b) True and estimated correlation functions averaged over 100 realizations.

lattice resolutions of 0.154 and 0.016 respectively. In this case, the coarse and fine scale layers have at least five basis functions per 0.8 and 0.08 spatial units respectively. Further we use LK and ELK-F with three layers composed of 14×14 , 37×37 , and 53×53 lattice grids over the spatial domain with 0.154, 0.077, and 0.038 resolutions respectively. LK is fit using `LatticeKrig` in R, and for both LK and ELK-F, we use a single layer-independent parameter κ . Additionally, we fit an approximation to the Gaussian process with Matérn covariance and smoothness $\nu = 1$ using the SPDE approach with `INLA` (Lindgren et al., 2011; Lindgren and Rue, 2015). The mean triangular mesh segment length is approximately 0.0064 within the spatial domain.

This gives in total four models: ELK-T, ELK-F, LK, and SPDE. In all cases we use a PC prior for the nugget variance satisfying the tail probability $P(\sigma_\epsilon > 1) = 0.01$, and for the SPDE model we use the prior derived in Fuglstad et al. (2019) on the effective range and spatial variance. The median effective range for the prior is a fifth of the spatial domain diameter, and the spatial standard deviation again satisfies $P(\sigma_S > 1) = 0.01$.

We use PC priors for the ELK-T and ELK-F spatial standard deviation also satisfying $P(\sigma_S > 1) = 0.01$, and use the effective range priors recommended in Section 3.2.

4.4 Results

For each realization and each of the Bayesian models, we generate 1,000 independent samples from the posterior distribution of Y (or conditional distribution in the case of LatticeKrig), estimate uncertainty in the parameters, and calculate covariance functions for each of the 100 independent parameter samples. We used only 100 parameter samples when generating covariance function draws since for each draw the corresponding precision matrix for u must be inverted, which is especially computationally intensive for LatticeKrig since it does not take advantage of `GMRFLib` library functions for factoring sparse symmetric positive definite matrices, and since ELK uses a simplified normalization scheme that precomputes normalization factors. In the case of LatticeKrig, we use the Hessian of the negative log likelihood to draw covariance parameter samples.

Figure 2b) shows the central correlation function estimate for each of the models together with the true correlation function. The ELK-T model approximates the true correlation function over all distances well, while the other models strongly underestimate the spatial correlation after distance of 0.1, and have negligible correlation after distances of approximately 0.5.

Pointwise predictive scoring rules calculated by distance from prediction location to nearest observation are shown in Figure 3. The RMSE and CRPS of ELK-T are the best in all of the distance bins. Differences in RMSE and CRPS among the models tend to increase as the distance to the nearest observation increases, but interestingly the differentiation is larger in the first bin than in the second bin. We believe this is due to the fact that ELK-T is able to capture the short range spatial correlation better than the three other models. The differences in RMSE and CRPS values for each model become increasingly large with longer distance to closest observation, indicating increasingly differing ability to accurately predict with longer distances.

Table 1 shows the summarized point and areal prediction scores. In terms of both

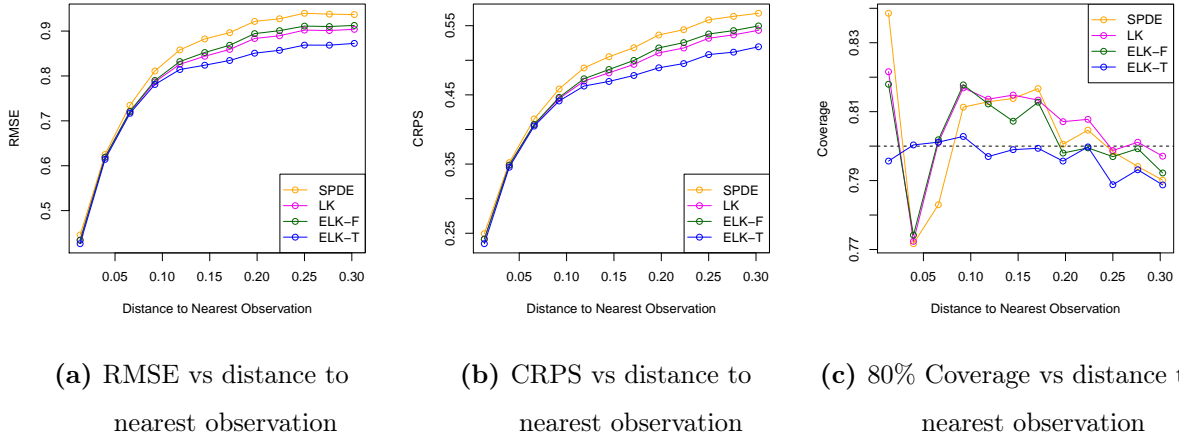


Figure 3: Scoring rules calculated in bins depending on distance to nearest observation. The scores are averaged over 100 simulations, and include (a) RMSE, (b) CRPS, and (c) 80% uncertainty interval coverage.

pointwise and areal scores, the SPDE predictions have the worst RMSE, CRPS, and coverage in all cases, although the coverage of all the models marches the nominal level of 80% in the pointwise case. The coverage of the SPDE model is especially poor near the observations, indicating its inability to simultaneously capture short and long scale spatial correlations. Figure 3 clearly demonstrates that even though SPDE achieves the correct nominal coverage overall, this is in spite of considerable over- and undercoverage depending on how far prediction locations are from the observations. There is also far more variability in coverage between bins for the SPDE model than ELK-T.

The runtime for the SPDE model is clearly the best. This is in part due to having an implementation that is pre-existing and optimized in the INLA package, whereas ELK-T and ELK-F were implemented manually using the comparatively slow `rgeneric` framework intended for prototyping new models and special cases in INLA. However, the fact that the SPDE model requires only two hyperparameters excluding any family likelihood hyperparameters, compared to the four required in this case for ELK-F and ELK-T, further improves its computational performance. LK had the longest runtimes in large part due to the implementation of the predictive distribution sampling when calculating SEs. Drawing the 1,000 samples took over 33 minutes on average for LK, whereas drawing the

	RMSE	CRPS	80% Cvg	Runtime (min.)
<i>Pointwise</i>				
SPDE	<i>0.605</i>	<i>0.342</i>	80	2.0
LK	0.594	0.334	80	<i>51.1</i>
ELK-F	0.594	0.335	80	9.4
ELK-T	0.587	0.329	80	12.1
<i>Areal</i>				
SPDE	<i>0.137</i>	<i>0.056</i>	<i>75</i>	2.0
LK	0.121	0.051	<i>77</i>	<i>51.1</i>
ELK-F	0.125	0.052	<i>77</i>	9.4
ELK-T	0.108	0.048	79	12.1

Table 1: Scoring rules averaged over 100 simulated realizations and over a regular 70×70 grid of prediction locations across the entire spatial domain and areally integrated over all nine cells in the 3×3 regular grid partitioning the domain. Averages are calculated for each of the considered models. *Italics* indicate worse performance, **boldface** indicates better performance.

same number of samples for the ELK-F model took under 2 minutes on average, and also included sampling over uncertainty in the hyperparameters.

The areal scores in Table 1 indicate a strong improvement from the SPDE model to ELK-F, and from ELK-F to ELK-T in terms of RMSE and CRPS. From the SPDE model to ELK-T, pointwise RMSE and CRPS scores improved respectively from 0.605 to 0.587 (3.0%) and from 0.342 to 0.329 (3.8%). However, in the integral prediction case, RMSE and CRPS scores improved respectively from 0.137 to 0.108 (21%) and from 0.056 to 0.048 (14%).

Table 5 in Section S.2 in the supplemental material shows that the improvements in areal predictions are even larger when considering only the central grid cell, but Table 6 in Section S.2 shows that there are improvements even when only the eight outer grid cells are considered. In summary, the results of this application show that multi-scale covariance models are essential both for accurate estimation of the covariance structure and for making predictions when the true covariance function is a mixture of short range and long range behavior.

5 Prevalence of secondary education completion

5.1 Analysis

We return to the data introduced in Section 2: counts of secondary education completion for young women aged 20-29 in Kenya in 2014 using the 2014 Kenya DHS. The 2014 Kenya DHS household survey contains responses from individuals sampled from 1,612 clusters in 47 counties, each of which except Nairobi and Mombasa (which are both entirely urban) contain both urban and rural strata, making 92 strata in total. These 47 counties subdivide the 8 geographical provinces in Kenya. The response at cluster c , conditional on the probability of secondary education completion, $p(\mathbf{x}_c)$ at cluster spatial location \mathbf{x}_c , $c = 1, \dots, 1612$, is modeled as, $Y(\mathbf{x}_c)|p(\mathbf{x}_c) \sim \text{Bin}(n_c, p(\mathbf{x}_c))$, where n_c is the total number of women aged 20-29 sampled in the cluster. The probability $p(\mathbf{x})$ is modeled on logit scale as,

$$\eta_c = \log\left(\frac{p(\mathbf{x}_c)}{1-p(\mathbf{x}_c)}\right) = \beta_0 + u(\mathbf{x}_c) + \beta^{\text{URB}}\mathbf{1}\{\mathbf{x}_c \in U\} + \epsilon_c, \quad c = 1, 2, \dots, 1612, \quad (1)$$

with intercept β_0 , spatial random effect $u(\mathbf{x}_c)$ with spatial variance σ_S^2 , fixed effect for urban areas β^{URB} , and mean zero iid Gaussian cluster random effect ϵ_c with variance σ_ϵ^2 . The indicator $\mathbf{1}\{\mathbf{x}_c \in U\}$ is 1 if \mathbf{x}_c is in U , the set of urban areas in Kenya, and 0 otherwise. LK is not applicable due to the binomial likelihood. We consider four alternatives for u : SPDE_u/SPDE_U and ELK-T_u/ELK-T_U models, where ‘U’ and ‘u’ respectively denote that urban effects are or are not included.

For ELK-T_u and ELK-T_U, the coarse lattice layer has 37km resolution, while the fine layer resolution was set to be 5km resolution in order to be able to capture sharp changes from urban localities to their rural surroundings. The SPDE model has an average triangular mesh segment length of approximately 15km across the spatial domain. The spatial domain diameter is approximately 1,445km, so the prior median effective range was set to be one fifth of that, or 289km, for the SPDE model and for the coarsest layer of the ELK models. We again place PC priors on the spatial and cluster variance parameters such that $P(\sigma_\epsilon > 1) = 0.01$ and $P(\sigma_S > 1) = 0.01$, except now the parameters should be interpreted on logit scale. All covariates except for the intercept are given noninformative

Gaussian priors with zero mean and 0.001 precision, and the intercept is given an improper $\text{Unif}(-\infty, \infty)$ prior.

Central estimates for the correlation and covariance functions of the fitted models are shown in Figure 4. Compared to the SPDE models, the ELK-T models incorporate more long scale spatial correlation while also modeling short scale correlations with more subtlety as shown by their long tailed covariance and correlation functions with sharp downward trends at small spatial distances. Including urbanicity as a covariate substantially reduces the spatial variance for all models, and also reduces the variance of the spatial nugget. We find that including an urban effect explains spatial variation at both short and long scales, because sharp changes due to urban/rural boundaries are accounted for, as well as long scale correlations across rural regions. We see this effect in the estimated correlation function of the ELK-T models, where the magnitude of the relatively sharp downward trend in correlation at small distances decreases when the urban effect is included, and where the long tail shortens slightly as well. Since the likelihood under Matérn correlation (or Matérn approximations like the SPDE model) is primarily affected by short correlation scales, the sharp changes in education due to changes in urbanicity rather than the long scale correlations induced by large areas being rural drive the correlation function estimate. Hence, including the urban effect in the SPDE model removes some of the otherwise unmodeled spatial correlation at short spatial scales, increasing the estimated effective range. It is worth noting, however, that even with an urban effect, the ELK-T_U model covariance estimates are still different to those in the SPDE_U model at both short and long scales.

In Figure 5 we give pixel level predictions at the 5km×5km resolution of secondary education prevalence as well as relative credible widths, which we define as credible widths divided by the corresponding central estimates. Areal predictions are created based on aggregation of pixel estimates weighted by population density as described in Equations (5-6) of Paige et al. (2020), except leaving out cluster effects by setting them to 0 rather than integrating over them as done in Equation (7) of Paige et al. (2020). Predictions and relative credible widths aggregated to the county and province levels are shown in Section S.3 in Figures 9 and 10. Tables of the county level and province predictions for the models

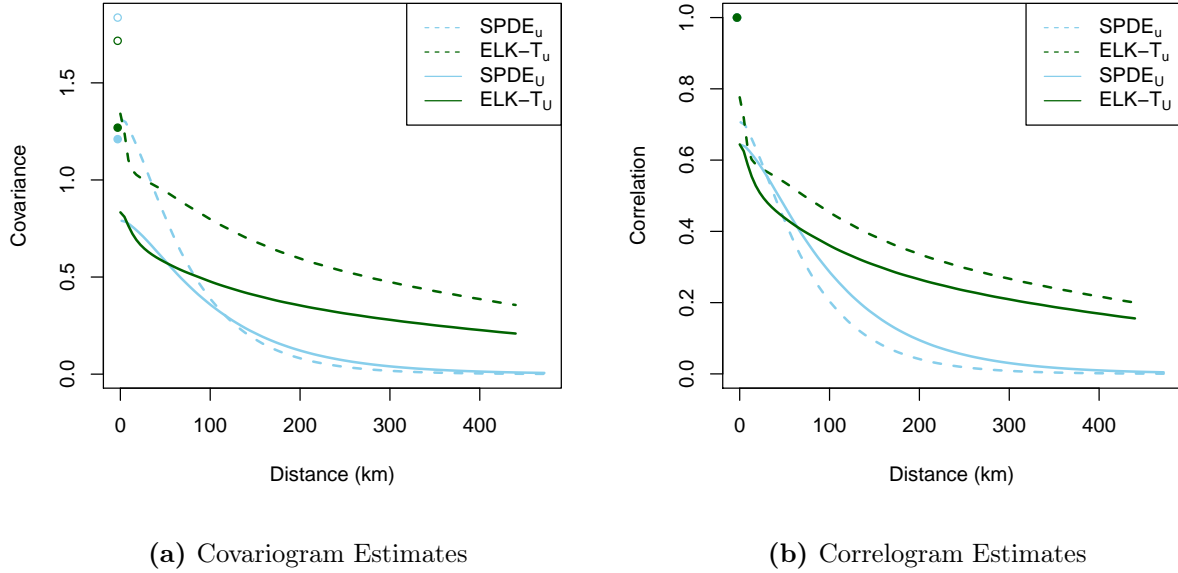


Figure 4: (a) Spatial covariance, and (b) correlation estimates. The spatial nugget is plotted as the dots at zero distance with the color corresponding to the model given in the legends. Filled dots are plotted for models including urban effects, and unfilled dots are plotted for models without urban effects.

with urban effects as well summary statistics for the model parameters are given in S.3 in Tables 7-9.

The pixel level predictions show nearly indistinguishable differences in predictions and uncertainties between the $SPDE_U$ and $ELK-T_U$ models, but much more significant differences in the predictions between the $SPDE_u$ and $ELK-T_u$ models. In particular, the $ELK-T_u$ model shows reduced spatial oversmoothing near urban areas, and higher uncertainties overall. These uncertainties reflect that an important confounder in urbanicity is not included as a covariate. The reduction in oversmoothing is especially noticeable in the north and east counties with large rural areas and spatially concentrated urban areas, although there are reductions in oversmoothing in other areas as well. The differences between the models without urban effects, and the similarities between the models with urban effects are further highlighted in the pair plots in Figure 6, which shows the predictions of the $SPDE_u$, $ELK-T_u$, and $SPDE_U$ models sequentially move towards the predictions of the $ELK-T_U$.

That the $SPDE_U$ and $ELK-T_U$ predictions are essentially indistinguishable lends credence to our predictions by showing they are robust to modeling assumptions. It also suggests that there is little identifiable spatial covariance at very short scales that is not already accounted for by urbanicity, and that the overall effect of remaining spatial confounders probably varies smoothly over medium to long spatial scales.

5.2 Validation

We use two different schemes to validate our models: leave one province out, and stratified, eight-fold cross validation (CV). In the leave one province out scheme, we calculate scoring rules based on the predicted distributions of the left out clusters in each of the 8 provinces consecutively, averaging the scores within each province, and then averaging the province scores to get the final reported scores. In the stratified, eight-fold CV, we randomly partition the set of clusters in each of the 92 strata (47 counties with each except of Nairobi and Mombasa begin urban and rural) into eight roughly equal sized folds. We make sure that for a given stratum, the difference between the number of clusters in each fold is different by at most one, and that which folds get more clusters than others is random. We choose eight folds since the smallest stratum has only eight clusters. The two different validation schemes give an idea of both short and long scale predictive errors due to the distribution of how far away left out clusters are from in sample observations. The leave one province out scheme better identifies long scale errors, and the stratified CV better identifies short and medium scale errors. The boundaries of the 8 provinces are plotted in Figure 5 along with county boundaries.

The results from the leave one province out and the stratified CV are given in Table 2. The ability of the $ELK-T$ model to account for more flexible spatial covariance structures than the $SPDE$ model leads to as good or better predictions as shown by RMSE, CRPS, and coverage standpoints, although the improvement is clearly greater when the urban effect is absent in the model. Improvements were especially obvious in the leave one province out CV, where long range correlations mattered more, and relative improvements were greater for CRPS than for RMSE. For leave one province out CV, RMSE improved by

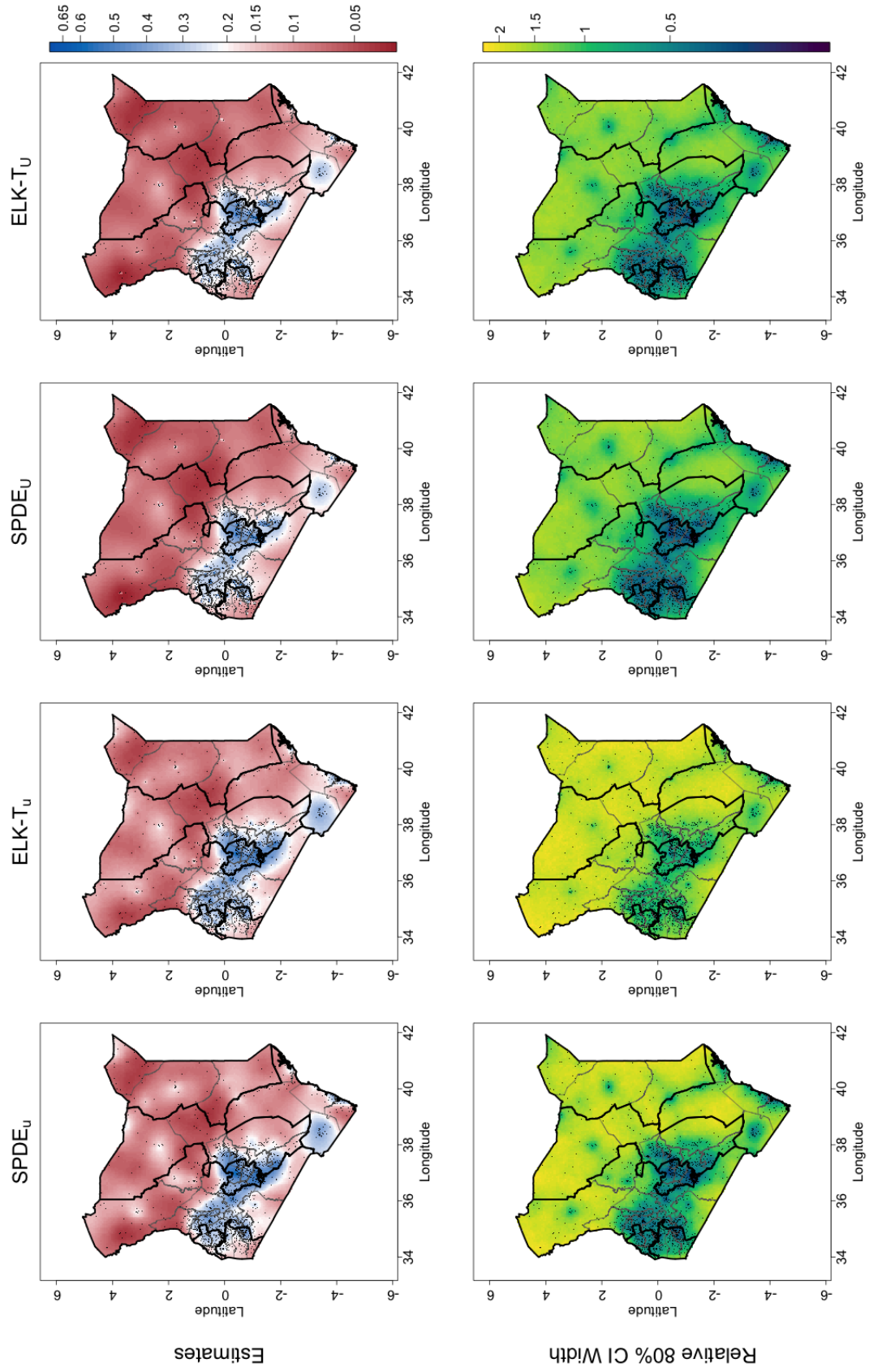


Figure 5: Central 5km×5km pixel level predictions (top row) and relative 80% credible interval widths (bottom row) of secondary education prevalence for young women in Kenya in 2014. Models with subscript ‘U’ and ‘u’ respectively do and do not include urban effects. Observation locations are plotted as black dots, provinces as thick black lines, and counties as thin gray lines.

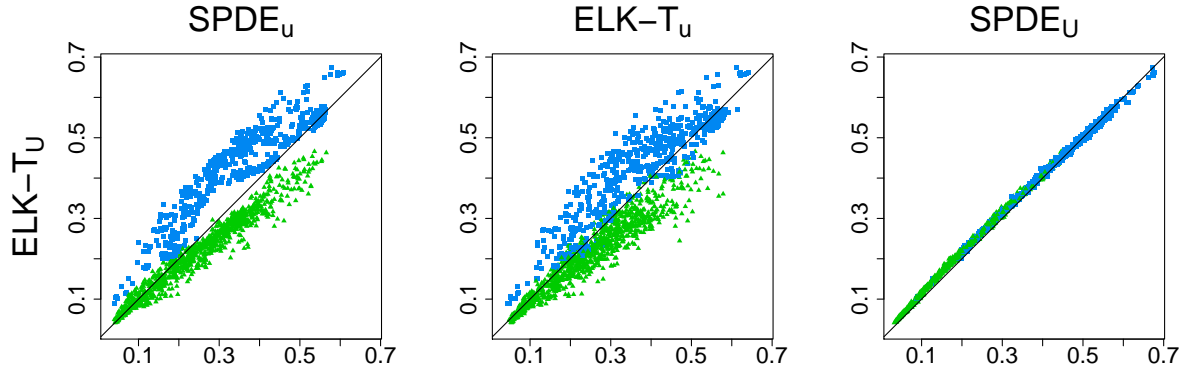


Figure 6: Pair plot of the cluster level estimates comparing the considered models’ estimates of secondary education prevalence to the ELK-T_U. The ‘▲’ symbols are rural clusters, while ‘■’ symbols are urban clusters.

1.7% when urban effects were not included in the SPDE and ELK-T models respectively, and by 0.4%, while CRPS improved by 3.1% when urban effects were not included, and by 1.7% otherwise. The SPDE_U model had the worst coverage with 74%, and both ELK-T models tied for the best coverage with 77%.

6 Discussion

The LK approach introduced by Nychka et al. (2015) attempts to address the question of how to flexibly model spatial covariance at different spatial scales in a computationally feasible way. However, in a spatial context where identifiability is already difficult, spatial confounders and the flexibility of LK when layer correlation ranges are allowed to independently vary further reduces identifiability. In this case, it may be necessary to account for prior information such as expert knowledge or to penalize model complexity, and it will certainly be important to integrate over parameter and hyperparameter uncertainty. By allowing for this without significant reductions in computational performance reductions, ELK’s Bayesian framework is a valuable extension over standard LK. It is not only more robust, but better accounts for multiple levels of uncertainty. Because of this, modelers might be less wary of fitting models with more complex covariance structure.

In ELK-T, due to the flexibility in choosing layer resolutions and the fact that its

	RMSE	CRPS	80% Cvg	Width
<i>Leave One Province Out</i>				
SPDE _u	<i>0.238</i>	<i>0.129</i>	76	0.52
SPDE _U	0.224	0.119	<i>74</i>	0.47
ELK-T _u	0.234	0.125	77	<i>0.53</i>
ELK-T _U	0.223	0.117	77	0.49
<i>Stratified 8-Fold</i>				
SPDE _u	<i>0.226</i>	<i>0.119</i>	73	0.46
SPDE _U	0.218	0.114	<i>72</i>	0.42
ELK-T _u	0.223	0.117	77	<i>0.49</i>
ELK-T _U	0.218	0.113	75	0.45

Table 2: Scoring rules calculated for each model using leave one province out and stratified 8-fold cross validation. Scores are averaged for each province, over urban areas, and over rural areas. *Italics* indicate worse performance, **boldface** indicates better performance.

effective range parameters are fit independently, ELK’s Bayesian framework is particularly important. We found ELK-T performed much better than ELK-F for the simulations we considered and the application since it was better able to efficiently model variation at contextually relevant spatial scales. In light of this, ELK’s use of Bayesian inference is all the more important.

Another advantage of ELK is that it eliminates the assumption of Gaussian responses by extending the LK framework to latent Gaussian models. This allows modeling responses with a diverse set of distributions, such as distributions in the exponential family, and even some others such as the betabinomial distribution, as long as priors on the latent model components are Gaussian. The implementation of ELK in INLA, avoids the computational expense of MCMC when integrating over parameter uncertainty. Moreover, we show that, computationally, ELK performs approximately better than LK when uncertainty in the predictions and covariance parameters is desired. ELK also has access to the suite of models that can be fit in INLA such as nonlinear random effects models for time series or covariates.

It is important to note that ELK-F requires $L + 1$ covariance parameters for L layers excluding variance parameters of the likelihood family, and ELK-T requires $2L$ covari-

ance parameters. Due to the exponential growth in the computation time requirements of optimization and integration over hyperparameter uncertainty as the number of hyperparameters grow, there is a limit to the number of layers for which computation is feasible. It is recommended for the number of hyperparameters in INLA models to be between 2 and 5, but certainly not exceeding 20 (Rue et al., 2017). Hence, computationally this method should typically use at most 4 layers for ELK-F and 2 or 3 layers for ELK-T for likelihoods without extra hyperparameters. It is certainly limited to 19 layers for ELK-F and 9 layers for ELK-T, which are far more than is necessary for both models. In general, for most practical purposes we see little reason to include more than 3 layers for ELK-T and 5 layers for ELK-F even if computation is feasible due to difficulty in model identification and lack of difference in predictive performance, although there may be some exceptions to this rule for ELK-F in particular since it can only model effective correlation ranges 2^{L-1} times larger than the range modeled by the finest layer.

In the simulation study, we show that the ability of LK and ELK to model spatial covariance flexibly can substantially improve predictive performance at both short and long scales. We find that, while short scale dependence is most important for point level predictions near observations, long scale dependence can matter more when making predictions in data sparse regions, and when making areal predictions.

When we apply the ELK model to a 2014 Kenya DHS dataset with information on the prevalence of secondary education for women aged 20-29 in 2014, we find substantial reductions in spatial oversmoothing relative to a SPDE model, especially when urbanicity was included as a covariate in the models. Evidence of short scale spatial confounding was present in the estimate of the spatial correlation function in the ELK model with no urban effect, indicating that ELK can make predictions more robust to spatial confounding as well as be indicative of the spatial scales at which spatial confounding is occurring. This in turn can suggest what variables should be included as covariates, and as an informal check for spatial confounding. In general, it is very difficult to tell whether an unmeasured covariate is confounding results, but ELK provides at least a modicum of insurance against this. Since DHS household surveys tend to consist of clusters that are spatially concentrated in

urban areas and sparsely distributed in rural areas, this is an application that ELK is well suited for.

Depending on the context, one may choose to select lattice resolutions that are independent of each other rather than changing by a factor of two from one layer to the next as in standard LK. In both the illustrative example and the application, we found that forcing each consecutive layer to have double the resolution along each dimension made modeling the fine and long scale changes simultaneously difficult from a computational perspective due to the number of hyperparameters and basis functions required. In such situations, we advocate for tailoring the resolutions of each lattice to enable them to model a set of effective ranges of interest.

SUPPLEMENTARY MATERIAL

Supplements: Section S.1 in the supplemental material provides details for how we calculate our fuzzy coverage intervals when computing coverage for discrete observations. Section S.2 and S.3 provide additional results for the simulation study and application respectively.

ELK code repository: Repository with R code for fitting the ELK model. Available on Github at: <https://github.com/paigejo/LK-INLA>.

References

- Banerjee, S., Gelfand, A. E., Finley, A. O., and Sang, H. (2008). Gaussian predictive process models for large spatial data sets. *Journal of the Royal Statistical Society, Series B*, 70:825–848.
- Cressie, N. and Johannesson, G. (2008). Fixed rank kriging for very large spatial data sets. *Journal of the Royal Statistical Society: Series B*, 70:209–226.
- Datta, A., Banerjee, S., Finley, A. O., and Gelfand, A. E. (2016a). Hierarchical nearest-neighbor Gaussian process models for large geostatistical datasets. *Journal of the American Statistical Association*, 111:800–812.

- Datta, A., Banerjee, S., Finley, A. O., and Gelfand, A. E. (2016b). On nearest-neighbor Gaussian process models for massive spatial data. *Wiley Interdisciplinary Reviews: Computational Statistics*, 8:162–171.
- DHS Program (2019). The DHS program – AIDS indicator surveys (AIS). <https://dhsprogram.com/What-We-Do/Survey-Types/AIS.cfm>.
- Filippone, M., Zhong, M., and Girolami, M. (2013). A comparative evaluation of stochastic-based inference methods for Gaussian process models. *Machine Learning*, 93:93–114.
- Finley, A. O., Sang, H., Banerjee, S., and Gelfand, A. E. (2009). Improving the performance of predictive process modeling for large datasets. *Computational Statistics and Data Analysis*, 53:2873–2884.
- Fuglstad, G.-A., Simpson, D., Lindgren, F., and Rue, H. (2019). Constructing priors that penalize the complexity of Gaussian random fields. *Journal of the American Statistical Association*, 114:445–452.
- Furrer, R., Genton, M. G., and Nychka, D. (2006). Covariance tapering for interpolation of large spatial datasets. *Journal of Computational and Graphical Statistics*, 15:502–523.
- Gelfand, A. E., Diggle, P., Guttorp, P., and Fuentes, M. (2010). *Handbook of spatial statistics*. CRC press.
- Gerber, F., de Jong, R., Schaepman, M. E., Schaepman-Strub, G., and Furrer, R. (2018). Predicting missing values in spatio-temporal remote sensing data. *IEEE Transactions on Geoscience and Remote Sensing*, 56:2841–2853.
- Geyer, C. J. and Meeden, G. D. (2005). Fuzzy and randomized confidence intervals and p-values. *Statistical Science*, 20:358–366.
- Gneiting, T. and Raftery, A. E. (2007). Strictly proper scoring rules, prediction, and estimation. *Journal of the American Statistical Association*, 102:359–378.
- Gómez-Rubio, V. (2020). *Bayesian inference with INLA*. CRC Press.

- Gramacy, R. B. and Apley, D. W. (2015). Local Gaussian process approximation for large computer experiments. *Journal of Computational and Graphical Statistics*, 24:561–578.
- Guhaniyogi, R. and Banerjee, S. (2018). Meta-kriging: Scalable Bayesian modeling and inference for massive spatial datasets. *Technometrics*, 60:430–444.
- Guinness, J. (2019). Spectral density estimation for random fields via periodic embeddings. *Biometrika*, 106:267–286.
- Guinness, J. and Fuentes, M. (2017). Circulant embedding of approximate covariances for inference from Gaussian data on large lattices. *Journal of computational and Graphical Statistics*, 26:88–97.
- Handcock, M. and Stein, M. (1993). A Bayesian analysis of kriging. *Technometrics*, 35:403–410.
- Heaton, M. J., Datta, A., Finley, A. O., Furrer, R., Guinness, J., Guhaniyogi, R., Gerber, F., Gramacy, R. B., Hammerling, D., Katzfuss, M., et al. (2019). A case study competition among methods for analyzing large spatial data. *Journal of Agricultural, Biological and Environmental Statistics*, 24:398–425.
- Hirano, T. and Yajima, Y. (2013). Covariance tapering for prediction of large spatial data sets in transformed random fields. *Annals of the Institute of Statistical Mathematics*, 65:913–939.
- Hyman, J. M. (1983). Accurate monotonicity preserving cubic interpolation. *SIAM Journal on Scientific and Statistical Computing*, 4:645–654.
- ICF International (2012). *Demographic and Health Survey Sampling and Household Listing Manual*. Calverton, Maryland, USA: ICF International.
- Katzfuss, M. (2017). A multi-resolution approximation for massive spatial datasets. *Journal of the American Statistical Association*, 112:201–214.
- Katzfuss, M. and Guinness, J. (2020). A general framework for Vecchia approximations of Gaussian processes. *Statistical Science*. To appear.

- Katzfuss, M., Guinness, J., Gong, W., and Zilber, D. (2018). Vecchia approximations of Gaussian-process predictions. *arXiv preprint arXiv:1805.03309*.
- Katzfuss, M. and Hammerling, D. (2017). Parallel inference for massive distributed spatial data using low-rank models. *Statistics and Computing*, 27:363–375.
- Kenya National Bureau of Statistics, Ministry of Health/Kenya, National AIDS Control Council/Kenya, Kenya Medical Research Institute, and National Council For Population And Development/Kenya (2015). *Kenya Demographic and Health Survey 2014*. Rockville, Maryland, USA.
- Knorr-Held, L. and Raßer, G. (2000). Bayesian detection of clusters and discontinuities in disease maps. *Biometrics*, 56:13–21.
- Konomi, B. A., Sang, H., and Mallick, B. K. (2014). Adaptive Bayesian nonstationary modeling for large spatial datasets using covariance approximations. *Journal of Computational and Graphical Statistics*, 23:802–829.
- Li, Z. R., Hsiao, Y., Godwin, J., Martin, B. D., Wakefield, J., and Clark, S. J. (2019). Changes in the spatial distribution of the under five mortality rate: small-area analysis of 122 DHS surveys in 262 subregions of 35 countries in Africa. *PLoS one*, 14. Published January 22, 2019.
- Lindgren, F. and Rue, H. (2015). Bayesian spatial modelling with R-INLA. *Journal of Statistical Software*, 63.
- Lindgren, F., Rue, H., and Lindström, J. (2011). An explicit link between Gaussian fields and Gaussian Markov random fields: the stochastic differential equation approach (with discussion). *Journal of the Royal Statistical Society, Series B*, 73:423–498.
- Neelon, B., Gelfand, A. E., and Miranda, M. L. (2014). A multivariate spatial mixture model for areal data: examining regional differences in standardized test scores. *Journal of the Royal Statistical Society: Series C (Applied Statistics)*, 63:737–761.

- Nychka, D., Bandyopadhyay, S., Hammerling, D., Lindgren, F., and Sain, S. (2015). A multiresolution Gaussian process model for the analysis of large spatial datasets. *Journal of Computational and Graphical Statistics*, 24:579–599.
- Nychka, D., Hammerling, D., Sain, S., and Lenssen, N. (2016). LatticeKrig: Multiresolution kriging based on Markov random fields. R package version 6.4.
- Paige, J., Fuglstad, G.-A., Riebler, A., and Wakefield, J. (2020). Design- and model-based approaches to small-area estimation in a low and middle income country context: Comparisons and recommendations. *Journal of Survey Statistics and Methodology*. To appear.
- Rue, H. and Follstad, T. (2001). GMRFLib: a C-library for fast and exact simulation of Gaussian Markov random fields. Technical report, SIS-2002-236.
- Rue, H. and Held, L. (2005). *Gaussian Markov Random Fields*, volume 104 of *Monographs on Statistics and Applied Probability*. Chapman & Hall/CRC, Boca Raton, FL.
- Rue, H., Martino, S., and Chopin, N. (2009a). Approximate Bayesian inference for latent Gaussian models by using integrated nested Laplace approximations. *Journal of the Royal Statistical Society: Series B (Statistical Methodology)*, 71:319–392.
- Rue, H., Martino, S., and Chopin, N. (2009b). Approximate Bayesian inference for latent Gaussian models using integrated nested Laplace approximations (with discussion). *Journal of the Royal Statistical Society, Series B*, 71:319–392.
- Rue, H., Riebler, A., Sørbye, S. H., Illian, J. B., Simpson, D. P., and Lindgren, F. K. (2017). Bayesian computing with INLA: a review. *Annual Review of Statistics and Its Application*, 4:395–421.
- Sang, H. and Huang, J. Z. (2012). A full scale approximation of covariance functions for large spatial data sets. *Journal of the Royal Statistical Society: Series B (Statistical Methodology)*, 74:111–132.

- Simpson, D., Rue, H., Riebler, A., Martins, T., and Sørbye, S. (2017). Penalising model component complexity: A principled, practical approach to constructing priors (with discussion). *Statistical Science*, 32:1–28.
- Sjöstedt-de Luna, S. and Young, A. (2003). The bootstrap and kriging prediction intervals. *Scandinavian Journal of Statistics*, 30:175–192.
- Stein, M. (1999). *Interpolation of Spatial Data: Some Theory for Kriging*. Springer.
- The World Bank (2019). Living standards measurement study (LSMS) | surveyunit. <http://surveys.worldbank.org/lsms>.
- Tuckwell, H. C. (2018). *Elementary applications of probability theory*. Routledge.
- UNICEF - Statistics and Monitoring (2012). Multiple Indicator Cluster Surveys (MICS). http://www.unicef.org/statistics/index_24302.html.
- United Nations (2020). *Sustainable Development Goals*. <http://sustainabledevelopment.un.org/owg.html>.
- USAID (2019). *Demographic and Health Surveys*. United States Agency for International Development, <http://www.dhsprogram.com>.
- Wagner, Z., Heft-Neal, S., Bhutta, Z. A., Black, R. E., Burke, M., and Bendavid, E. (2018). Armed conflict and child mortality in Africa: a geospatial analysis. *The Lancet*.
- Wakefield, J., Fuglstad, G.-A., Riebler, A., Godwin, J., Wilson, K., and Clark, S. (2019). Estimating under five mortality in space and time in a developing world context. *Statistical Methods in Medical Research*, 28:2614–2634.
- Wendland, H. (1995). Piecewise polynomial, positive definite and compactly supported radial functions of minimal degree. *Advances in Computational Mathematics*, 4:389–396.
- Zilber, D. and Katzfuss, M. (2019). Vecchia-Laplace approximations of generalized Gaussian processes for big non-Gaussian spatial data. *arXiv preprint arXiv:1906.07828*.

Appendix A: Relevant Correlation Scales for Spatial Integration

Long-range correlations are especially important when calculating predictions of certain areal averages. With a ‘back of the envelope’ calculation one can calculate the variance of a predicted spatial integral over a disk with radius R . Let $\hat{r}(d)$ be the estimated covariance, and let $r(d)$ be the true covariance such that,

$$\hat{r}(d) = r(d) + e(d),$$

so e is the error in the covariance estimate as a function of distance. Then if we denote the disk by A , and the true spatial field with $g(\mathbf{x})$, the variance of our spatial integral under the predictive distribution is:

$$\begin{aligned} \widehat{\text{Var}}(g(A)) &= \int_A \int_A \widehat{\text{Cov}}(\mathbf{u}, \mathbf{v}) \, d\mathbf{u} \, d\mathbf{v} \\ &= \int_A \int_A r(\|\mathbf{u} - \mathbf{v}\|) + e(\|\mathbf{u} - \mathbf{v}\|) \, d\mathbf{u} \, d\mathbf{v} \\ &= \text{Var}(g(A)) + \int_A \int_A e(\|\mathbf{u} - \mathbf{v}\|) \, d\mathbf{u} \, d\mathbf{v}. \end{aligned}$$

Let D be the random distance between any two points chosen in the disk with independent uniform distributions. Then Tuckwell (2018) shows the density of D is:

$$p_D(d) = \begin{cases} \frac{4d}{\pi R^2} \left(\arccos\left(\frac{d}{2R}\right) - \frac{d}{2R} \sqrt{1 - \left(\frac{d}{2R}\right)^2} \right), & 0 \leq d \leq 2R \\ 0, & \text{otherwise.} \end{cases}$$

Hence,

$$\widehat{\text{Var}}(g(A)) = \text{Var}(g(A)) + \int_0^{2R} e(D) \cdot \frac{4d}{\pi R^2} \left(\arccos\left(\frac{d}{2R}\right) - \frac{d}{2R} \sqrt{1 - \left(\frac{d}{2R}\right)^2} \right) dD.$$

Fig. 7 shows that the density $p_D(d)$ roughly parabolic with peak just under R (approximately $0.834R$), and has zeros at 0 and $2R$. Because of this, errors in very short and very long-range correlations are less relevant than errors in the assumed correlation function at the spatial scale near the radius of the area over which we integrate, R , when calculating

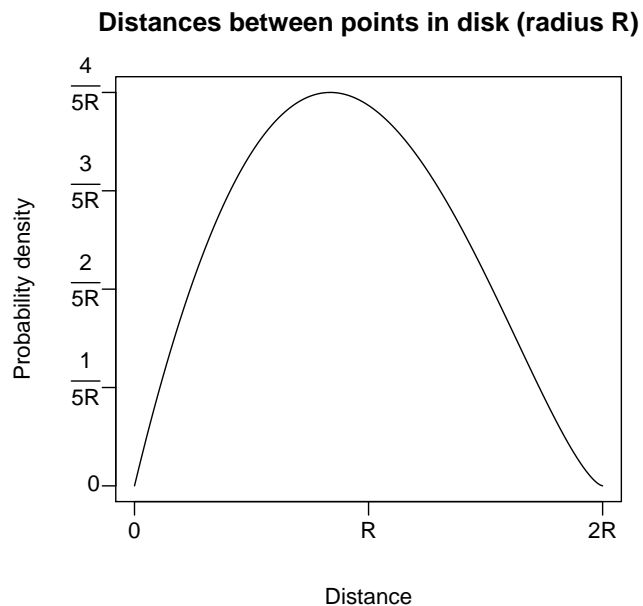


Figure 7: The distribution of distances between points uniformly distributed on a disk of radius R .

predictive uncertainties. This is of course not the full story, since the covariance structure conditional on the data will not be so neatly stationary and isotropic, and will likely have shorter spatial range. At the same time, we believe this shows greater emphasis must be placed on long range spatial correlations when producing area level predictions, especially in large areas.

Appendix B: ELK Sparse Matrix Computations

The computational performance of our implementation of ELK within *inla* is almost entirely determined by how quickly the sparse precision matrix of the basic coefficients \mathbf{c} can be generated. As such, we precompute any information for this task that will improve the performance. Recall that thus basis coefficients for each layer follow independent SAR

models with mean zero Gaussian distribution, $\mathbf{c}_l \sim \text{MVN}(\mathbf{0}, \alpha_l \sigma_S^2 \mathbf{B}_l^{-1} \mathbf{B}_l^{-T})$, with,

$$\mathbf{B}_{l,i,j} = \begin{cases} 4 + \kappa_l^2, & i = j \\ -1, & i \in N_l(j) \\ 0, & \text{otherwise,} \end{cases}$$

where $N_l(j)$ is this set of indices of lattice knots in layer l neighboring lattice knot i . The precision matrix for layer l , \mathbf{Q}_l , can therefore be represented as,

$$\mathbf{Q}_l = \frac{\omega_l}{\alpha_l \sigma_S^2} \left(\kappa_l^4 \mathbf{I}_{m(l)} - \kappa_l^2 (\mathbf{D}^l + (\mathbf{D}^l)^T) + (\mathbf{D}^l)^T \mathbf{D}^l \right),$$

for matrices,

$$\begin{aligned} \mathbf{D}^l &= \mathbf{D}_x^l + \mathbf{D}_y^l \\ \mathbf{D}_x^l &= \mathbf{I}_{m_y(l)} \otimes \nabla_{m_x(l)}^2 \\ \mathbf{D}_y^l &= \mathbf{I}_{m_x(l)} \otimes \nabla_{m_y(l)'}^2 \end{aligned}$$

where $m_x(l)$ and $m_y(l)$ are the number of basis functions in the horizontal and vertical directions of layer l , $\mathbf{I}_{m_x(l)}$ and $\mathbf{I}_{m_y(l)}$ are $m_x(l) \times m_x(l)$ and $m_y(l) \times m_y(l)$ identity matrices respectively, and ‘ \otimes ’ denotes the Kronecker product. Note that the variance normalization factor ω_l is a function of κ_l , although we leave out this dependence in the notation for simplicity. We can therefore precompute $\mathbf{D}^l + (\mathbf{D}^l)^T$ and $(\mathbf{D}^l)^T \mathbf{D}^l$ in order to calculate \mathbf{Q}_l as quickly as possible for each chosen value of κ_l .

Since there is no exact closed form solution for the functions $f_l : \kappa_l \mapsto \omega_l$, $l = 1, \dots, L$, they are approximated using monotonic smoothing splines (Hyman, 1983) fit on a log-log scale over a set of reasonable effective ranges for each layer. Throughout this paper, the effective ranges used for fitting f_1 vary from a fifth of the first layer lattice width to the diameter of the spatial domain, and the effective ranges used when fitting subsequent f_l shrink proportionally with the corresponding lattice widths. Hence, if w is the diameter of the spatial domain, then each f_l is fit with effective ranges varying in the interval $\left(\frac{\delta_l}{5}, \frac{\delta_l}{5} \cdot \frac{w}{5}\right)$. We find the splines are nearly linear, so estimates of f_l are very accurate even somewhat outside of the interval used for fitting.

Supplementary Materials for Bayesian Multiresolution Modeling of Georeferenced Data

John Paige *

Department of Statistics, University of Washington,
Geir-Arne Fuglstad

Department of Mathematical Sciences, NTNU,
Andrea Riebler

Department of Mathematical Sciences, NTNU,
and Jon Wakefield

Departments of Statistics and Biostatistics, University of Washington

May 27, 2020

S.1 Fuzzy Coverage and Interval Width for Count Data

For observation i , let $Q_{\alpha/2}^i$ and $Q_{1-\alpha/2}^i$ be the discrete $\alpha/2$ and $1-\alpha$ quantiles of a predictive distribution for empirical proportion y_i so that $p_l \equiv P(y_i < Q_{\alpha/2}^i) \leq \alpha/2$ and $p_u \equiv P(y_i > Q_{1-\alpha/2}^i) \leq \alpha/2$. Then $P(Q_{\alpha/2}^i \leq y_i \leq Q_{1-\alpha/2}^i) \geq 1 - \alpha$. We will show how to calculate coverage using fuzzy coverage intervals in order to achieve coverage closer to the nominal rate.

Rather than using a fixed uncertainty interval when performing hypothesis tests for discrete data, randomized tests involving randomized uncertainty intervals are the uniformly most powerful (UMP) one tailed and UMP unbiased (UMPU) two-tailed tests (Lehmann and Romano, 2005, Chapters 3 and 4). In a randomized test, we could randomly reject that y_i is in our interval if y_i is equal to $Q_{\alpha/2}^i$ or $Q_{1-\alpha/2}^i$ in such a way as to obtain equal tail rejection probabilities and achieve $1 - \alpha$ coverage. In the lower tail case, we have:

$$\begin{aligned} \alpha/2 &= P(\text{reject } y_i \text{ at lower tail}) \\ &= P(y_i < Q_{\alpha/2}^i) + P(\text{reject } y_i \text{ at lower tail, } y_i = Q_{\alpha/2}^i). \end{aligned}$$

*John Paige was supported by The National Science Foundation Graduate Research Fellowship Program under award DGE-1256082, and Jon Wakefield was supported by the National Institutes of Health under award R01CA095994.

This implies we can choose $P(\text{reject } y_i \mid y_i = Q_{\alpha/2}^i)$ and $P(\text{reject } y_i \mid y_i = Q_{1-\alpha/2}^i)$ in the following way in order to achieve the correct coverage, assuming the predictive distribution is correct:

$$\alpha/2 = p_l + P(\text{reject } y_i \mid y_i = Q_{\alpha/2}^i) \cdot P(y_i = Q_{\alpha/2}^i) \quad (9)$$

$$\alpha/2 = p_u + P(\text{reject } y_i \mid y_i = Q_{1-\alpha/2}^i) \cdot P(y_i = Q_{1-\alpha/2}^i). \quad (10)$$

Since the resulting coverage intervals are random, different statisticians may randomly report different results. To eliminate this possibility, we will follow the proposal of Geyer and Meeden (2005) to use fuzzy set theory to compute fuzzy intervals. To do this, we calculate the membership function for U^i , the *fuzzy* uncertainty interval for the i th observation, as:

$$I_{U^i}(y_i) = \begin{cases} 1, & Q_{\alpha/2}^i < y_i < Q_{1-\alpha/2}^i \\ P(\text{reject } y_i \mid y_i = Q_{\alpha/2}^i), & y_i = Q_{\alpha/2}^i \\ P(\text{reject } y_i \mid y_i = Q_{1-\alpha/2}^i), & y_i = Q_{1-\alpha/2}^i \\ 0, & \text{otherwise,} \end{cases} \quad (11)$$

where $P(\text{reject } y_i \mid y_i = Q_{\alpha/2}^i)$ and $P(\text{reject } y_i \mid y_i = Q_{1-\alpha/2}^i)$ are calculated from Eqs. (9-10). We then calculate coverage for a single observation as the membership function of the fuzzy interval,

$$\text{Cvg}(y_i) = I_{U^i}(y_i),$$

in order to achieve the nominal coverage deterministically.

To calculate fuzzy credible interval width, we modify the standard width calculations by accounting for the rejection probabilities in Eqs. (9-10):

$$\text{Width}(y_i) = Q_{1-\alpha/2}^i - Q_{\alpha/2}^i - \frac{1}{N_i} \left[P(\text{reject } y_i \mid y_i = Q_{\alpha/2}^i) + P(\text{reject } y_i \mid y_i = Q_{1-\alpha/2}^i) \right],$$

where $\frac{1}{N_i}$ is the width of the discrete steps the interval width could increase by if fuzzy intervals were not used.

S.2 Assessing Performance Under Multiscale Dependence: Additional Results

In addition to the results for the simulation study shown in the main text, we also calculated scores for the predictions integrated over the nine grid cells throughout the domain, averaged over the 100 realizations for the single central grid cell without observations, and for the eight other grid cells containing observations. These average scores are respectively given in Tables 5 and 6. Figure depicts the data domain and knots for the three lattice layer ELK model.

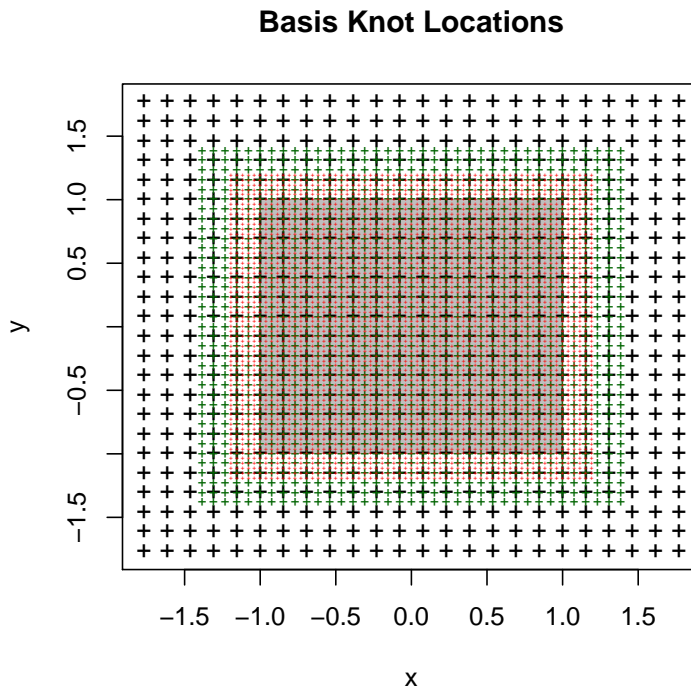


Figure 8: An example of a set of three lattice layers for the given $[-1, 1] \times [-1, 1]$ data domain represented by the shaded region. The ‘+’ signs represent the knot points where the basis functions are centered: large black symbols representing the coarsest, first layer, medium green symbols representing the second layer, and small red symbols representing the last, finest layer.

	RMSE	CRPS	80% Cvg	CI Width
SPDE	<i>0.37</i>	<i>0.21</i>	<i>60</i>	0.61
LK	0.31	0.18	75	0.68
ELK-F	0.33	0.19	67	0.64
ELK-T	0.27	0.16	76	0.66

Table 5: Scoring rules for predictions of integrals of the latent field over the center most of the nine cells in the 3×3 regular grid. The scoring rules are averaged over 100 simulated realizations and are calculated for each of the considered models. *Italics* indicate worse performance, **boldface** indicates better performance.

	RMSE	CRPS	80% Cvg	CI Width
SPDE	<i>0.066</i>	<i>0.037</i>	<i>77</i>	<i>0.16</i>
LK	0.062	0.035	77	0.15
ELK-F	0.063	0.035	78	0.15
ELK-T	0.061	0.034	79	0.15

Table 6: Scoring rules for predictions of integrals of the latent field over the outer most eight of the nine cells in the 3×3 regular grid. The scoring rules are averaged over 100 simulated realizations and are calculated for each of the considered models. *Italics* indicate worse performance, **boldface** indicates better performance.

Parameter	Est	SD	Q10	Q50	Q90
<i>SPDE_U</i>					
Intercept	-2.392	0.262	-2.381	-2.724	-2.073
Urban	0.927	0.067	0.927	0.841	1.012
Total Var	1.244	0.233	0.941	1.194	1.609
Spatial Var	0.824	0.227	0.555	0.775	1.167
Cluster Var	0.421	0.052	0.342	0.419	0.510
Total SD	1.111	0.103	0.970	1.092	1.268
Spatial SD	0.899	0.124	0.745	0.880	1.080
Cluster SD	0.647	0.040	0.585	0.647	0.714
Range (km)	203	43	154	196	267
<i>ELK-T_U</i>					
Intercept	-2.433	0.316	-2.836	-2.416	-2.055
Urban	0.930	0.067	0.844	0.930	1.016
Total Var	1.298	0.290	0.977	1.206	1.705
Spatial Var	0.870	0.277	0.556	0.780	1.283
Cluster Var	0.428	0.053	0.354	0.426	0.487
Total SD	1.132	0.126	0.988	1.098	1.306
Spatial SD	0.921	0.146	0.746	0.883	1.133
Cluster SD	0.653	0.041	0.595	0.653	0.698
Range ₁ (km)	571	451	315	375	1365
Range ₂ (km)	135	51	78	118	199
α_1	0.480	0.209	0.241	0.538	0.786
α_2	0.520	0.209	0.214	0.462	0.759

Table 7: Parameter posterior estimates, standard deviations, and 80% CIs for the given models fit to secondary education completion KDHS data for women aged 20-29 in Kenya in 2014.

S.3 Prevalence of Secondary Education in Kenya: Survey Design and Additional Results

The KHDS follows a typical DHS design: it is a stratified, two-stage design, where the first stage consists of selecting enumeration areas (EAs) from each stratum with probability proportional to size (PPS) sampling, where the ‘size’ used to calculate sampling probabilities is based on the number of households in each EA. The second stage consists of selecting 25 households randomly within each EA, (Kenya National Bureau of Statistics, Ministry of Health/Kenya, National AIDS Control Council/Kenya, Kenya Medical Research Institute, and National Council For Population And Development/Kenya, 2015; ICF International, 2012). Strata are based on the 47 counties crossed with official urban/rural designations, where two counties, Nairobi and Mombasa, are entirely urban, making 92 strata in total. 1,612 clusters are sampled from the 96,251 EAs in Kenya that are based on the 2009 Kenya Population and Housing Census (Kenya National Bureau Of Statistics, 2014).

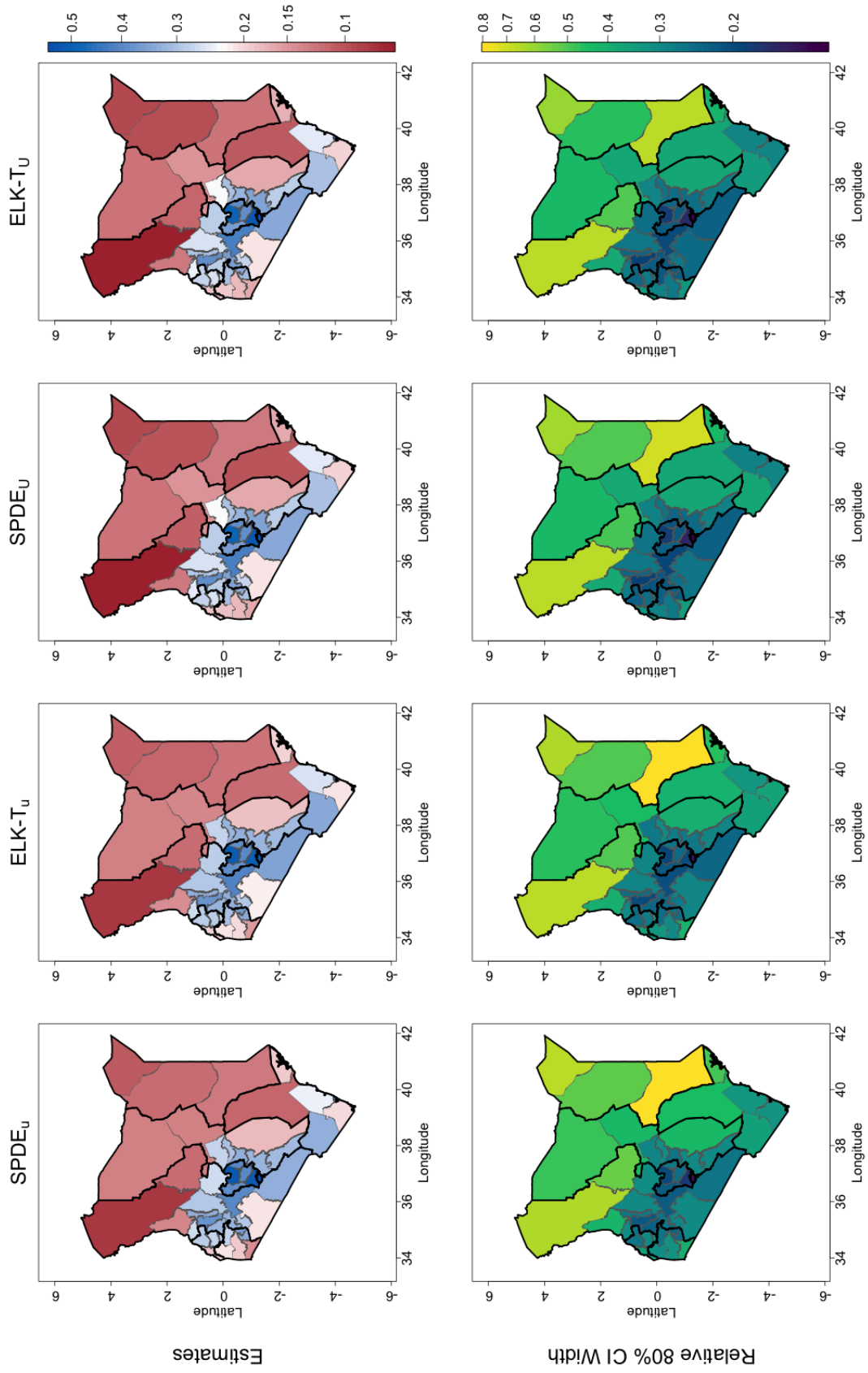


Figure 9: Central county level predictions (top row) and relative 80% credible interval widths (bottom row) of secondary education prevalence for young women in Kenya in 2014. Models with subscript ‘u’ and ‘U’ respectively do and do not include urban effects. Province and county borders are shown as black and grey lines respectively.

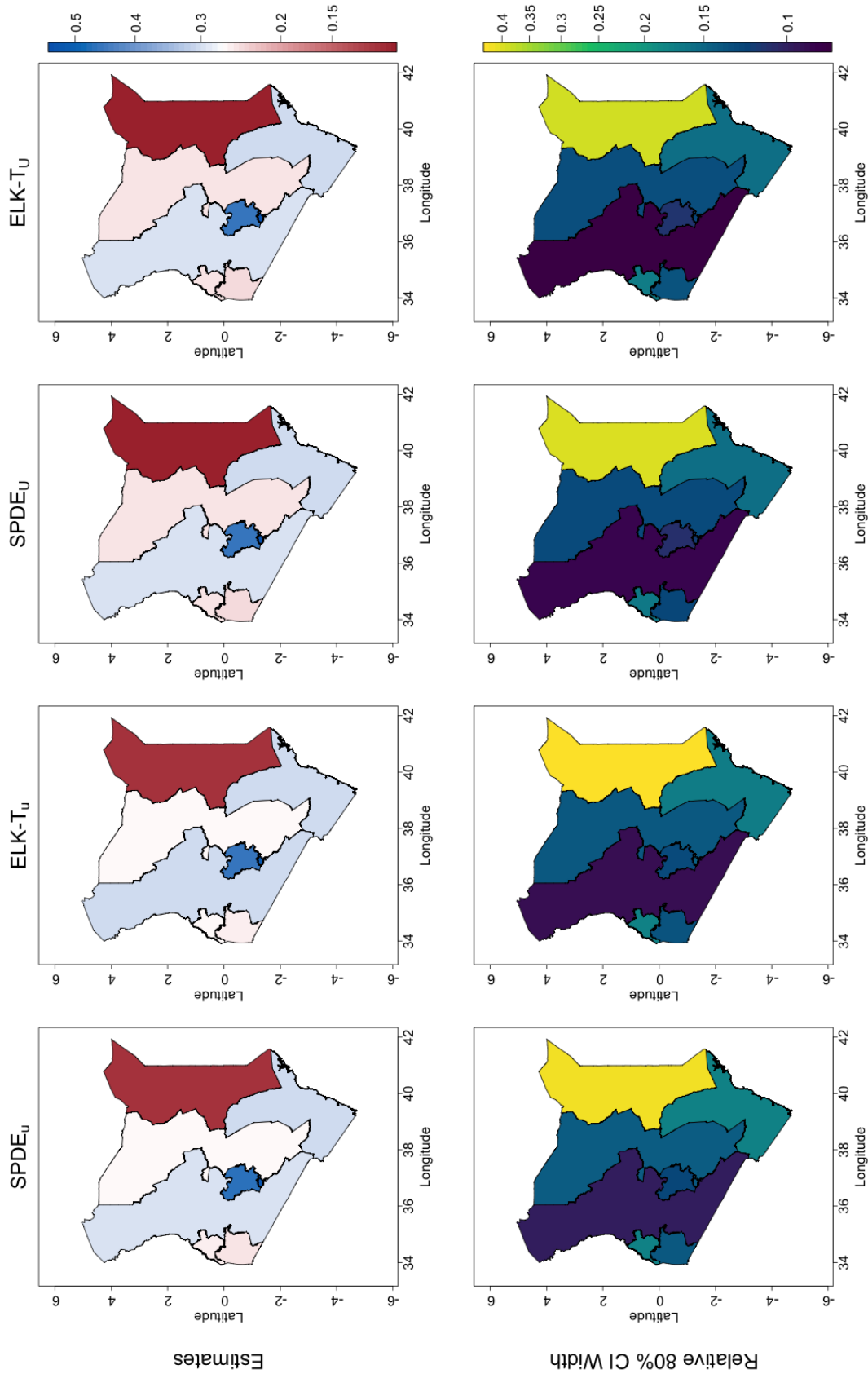


Figure 10: Central province level predictions (top row) and relative 80% credible interval widths (bottom row) of secondary education prevalence for young women in Kenya in 2014. Models with subscript ‘u’ and ‘U’ respectively do and do not include urban effects.

Province	<i>SPDE_U</i>			<i>ELK-T_U</i>		
	Est	Q10	Q90	Est	Q10	Q90
Central	0.4578	0.4331	0.4826	0.4566	0.4326	0.4813
Coast	0.3030	0.2791	0.3276	0.3047	0.2814	0.3287
Eastern	0.2542	0.2377	0.2706	0.2556	0.2381	0.2734
Nairobi	0.5403	0.5082	0.5727	0.5391	0.5066	0.5706
North Eastern	0.1059	0.0856	0.1281	0.1046	0.0845	0.1261
Nyanza	0.2429	0.2277	0.2578	0.2432	0.2278	0.2598
Rift Valley	0.2935	0.2808	0.3066	0.2940	0.2809	0.3065
Western	0.2492	0.2283	0.2696	0.2489	0.2291	0.2684

Table 8: Province predictions and 80% CIs for prevalence of secondary education completion for women aged 20-29 in Kenya in 2014.

Table 9: County level predictions and 80% CIs for prevalence of secondary education completion for women aged 20-29 in Kenya in 2014.

County	<i>SPDE_U</i>			<i>ELK-T_U</i>		
	Est	Q10	Q90	Est	Q10	Q90
Baringo	0.2615	0.2267	0.2977	0.2607	0.2256	0.2983
Bomet	0.2768	0.2418	0.3128	0.2765	0.2408	0.3131
Bungoma	0.2734	0.2422	0.3063	0.2748	0.2440	0.3082
Busia	0.1810	0.1513	0.2103	0.1806	0.1524	0.2122
Elgeyo Marakwet	0.2935	0.2591	0.3292	0.2953	0.2609	0.3292
Embu	0.3183	0.2800	0.3568	0.3205	0.2829	0.3590
Garissa	0.1250	0.0829	0.1719	0.1225	0.0824	0.1692
Homa Bay	0.1795	0.1552	0.2032	0.1803	0.1558	0.2067
Isiolo	0.1467	0.1195	0.1757	0.1483	0.1216	0.1765
Kajiado	0.3372	0.2972	0.3755	0.3394	0.3012	0.3770
Kakamega	0.2573	0.2263	0.2916	0.2560	0.2248	0.2882
Kericho	0.3510	0.3127	0.3891	0.3513	0.3142	0.3889
Kiambu	0.5182	0.4776	0.5577	0.5164	0.4742	0.5565
Kilifi	0.2461	0.2113	0.2816	0.2471	0.2119	0.2841
Kirinyaga	0.3883	0.3461	0.4285	0.3879	0.3458	0.4331
Kisii	0.3039	0.2715	0.3396	0.3055	0.2709	0.3417
Kisumu	0.3057	0.2714	0.3416	0.3041	0.2705	0.3384
Kitui	0.1631	0.1335	0.1942	0.1652	0.1352	0.1958
Kwale	0.1978	0.1696	0.2278	0.1999	0.1726	0.2298
Laikipia	0.2856	0.2480	0.3227	0.2862	0.2519	0.3237
Lamu	0.1647	0.1297	0.2011	0.1684	0.1317	0.2102

Table 9: County level predictions and 80% CIs for prevalence of secondary education completion for women aged 20-29 in Kenya in 2014. (*continued*)

County	<i>SPDE_U</i>			<i>ELK-T_U</i>		
	Est	Q10	Q90	Est	Q10	Q90
Machakos	0.3514	0.3086	0.3951	0.3515	0.3073	0.3977
Makueni	0.2821	0.2421	0.3226	0.2845	0.2448	0.3267
Mandera	0.0945	0.0659	0.1242	0.0943	0.0655	0.1256
Marsabit	0.1238	0.0981	0.1520	0.1223	0.0955	0.1514
Meru	0.2330	0.2001	0.2661	0.2345	0.2016	0.2682
Migori	0.1676	0.1398	0.1970	0.1689	0.1399	0.1973
Mombasa	0.4215	0.3761	0.4680	0.4241	0.3809	0.4665
Murang'a	0.3897	0.3465	0.4326	0.3859	0.3419	0.4289
Nairobi	0.5403	0.5082	0.5727	0.5391	0.5066	0.5706
Nakuru	0.4185	0.3780	0.4587	0.4196	0.3797	0.4607
Nandi	0.2799	0.2504	0.3097	0.2777	0.2487	0.3093
Narok	0.2091	0.1817	0.2364	0.2094	0.1837	0.2370
Nyamira	0.3278	0.2894	0.3658	0.3267	0.2855	0.3659
Nyandarua	0.3586	0.3187	0.4004	0.3599	0.3208	0.3986
Nyeri	0.4863	0.4413	0.5294	0.4878	0.4427	0.5330
Samburu	0.1101	0.0847	0.1383	0.1130	0.0831	0.1438
Siaya	0.1871	0.1609	0.2149	0.1876	0.1618	0.2150
Taita Taveta	0.3038	0.2509	0.3631	0.3040	0.2499	0.3599
Tana River	0.1026	0.0845	0.1233	0.1030	0.0842	0.1230
Tharaka-Nithi	0.3024	0.2638	0.3435	0.3037	0.2643	0.3428
Trans-Nzoia	0.2465	0.2136	0.2826	0.2473	0.2137	0.2810
Turkana	0.0707	0.0495	0.0965	0.0714	0.0504	0.0963
Uasin Gishu	0.3883	0.3516	0.4239	0.3885	0.3506	0.4248
Vihiga	0.2699	0.2341	0.3053	0.2694	0.2347	0.3060
Wajir	0.0996	0.0755	0.1254	0.0982	0.0745	0.1241
West Pokot	0.1278	0.1032	0.1525	0.1291	0.1052	0.1551

References

- Geyer, C. J. and Meeden, G. D. (2005). Fuzzy and randomized confidence intervals and p-values. *Statistical Science*, 20:358–366.
- ICF International (2012). *Demographic and Health Survey Sampling and Household Listing Manual*. Calverton, Maryland, USA: ICF International.
- Kenya National Bureau of Statistics, Ministry of Health/Kenya, National AIDS Control Council/Kenya, Kenya Medical Research Institute, and National Council For Population

And Development/Kenya (2009). *The 2009 Kenya Population and Housing Census Volume IC: Population Distribution by Age, Sex, and Administrative Units*. Nairobi: Kenya National Bureau of Statistics.

Kenya National Bureau of Statistics, Ministry of Health/Kenya, National AIDS Control Council/Kenya, Kenya Medical Research Institute, and National Council For Population And Development/Kenya (2015). *Kenya Demographic and Health Survey 2014*. Rockville, Maryland, USA.

Lehmann, E. L. and Romano, J. P. (2005). *Testing Statistical Hypotheses*. Springer Texts in Statistics, 3rd. ed. edition.